

## PHENIX Muon Arms

H. Akikawa<sup>k</sup> A. Al-Jamel<sup>m</sup> J.B. Archuleta<sup>1</sup> J.R. Archuleta<sup>1</sup>  
R. Armendariz<sup>m</sup> V. Armijo<sup>1</sup> T.C. Awes<sup>o</sup> A. Baldisseri<sup>v</sup>  
A.B. Barker<sup>a</sup> P.D. Barnes<sup>1</sup> B. Bassalleck<sup>n</sup> S. Batsouli<sup>e</sup>  
J. Behrendt<sup>n</sup> F.G. Bellaiche<sup>o</sup> A.W. Bland<sup>a</sup> M. Bobrek<sup>o</sup>  
J.G. Boissevain<sup>1</sup> H. Borel<sup>v</sup> M.L. Brooks<sup>1</sup> A.W. Brown<sup>a</sup>  
D.S. Brown<sup>m</sup> N. Bruner<sup>n</sup> M.M. Cafferty<sup>1</sup> T.A. Carey<sup>1</sup>  
J.-S. Chai<sup>i</sup> L.L. Chavez<sup>n</sup> S. Chollet<sup>q</sup> R.K. Choudhury<sup>b</sup>  
M.S. Chung<sup>j</sup> V. Cianciolo<sup>o</sup> D.J. Clark<sup>1</sup> Y. Cobigo<sup>v</sup>  
C.M. Dabrowski<sup>c</sup> A. Debraine<sup>q</sup> J. DeMoss<sup>n</sup> B.V. Dinesh<sup>b</sup>  
J.L. Drachenberg<sup>a</sup> O. Drapier<sup>q</sup> M.A. Echave<sup>1</sup>  
Y.V. Efremenko<sup>x,o</sup> H. En'yo<sup>t,k</sup> D.E. Fields<sup>n</sup> F. Fleuret<sup>q</sup>  
J. Fried<sup>c</sup> E. Fujisawa<sup>y</sup> H. Funahashi<sup>k</sup> S. Gadrat<sup>r</sup> F. Gastaldi<sup>q</sup>  
T.F. Gee<sup>o</sup> A. Glenn<sup>x</sup> G. Gogiberidze<sup>x</sup> M. Gonin<sup>q</sup> J. Gosset<sup>v</sup>  
R. Granier de Cassagnac<sup>q</sup> R.H. Hance<sup>a</sup> G.W. Hart<sup>1</sup>  
N. Hayashi<sup>t</sup> S. Held<sup>x</sup> J.S. Hicks<sup>o</sup> J.C. Hill<sup>f</sup> R. Hoade<sup>c</sup>  
B. Hong<sup>j</sup> A. Hoover<sup>m</sup> C.T. Hunter<sup>a</sup> D.E. Hurst<sup>o</sup> T. Ichihara<sup>t,u</sup>  
K. Imai<sup>k</sup> L.Davis Isenhower<sup>a</sup> L.Donald Isenhower<sup>a</sup>  
M. Ishihara<sup>t,u</sup> W.Y. Jang<sup>j</sup> J. Johnson<sup>o</sup> D. Jouan<sup>p</sup>  
Y. Kamyshkov<sup>x,o</sup> J.H. Kang<sup>z</sup> S.S. Kapoor<sup>b</sup> D.J. Kim<sup>z</sup>  
D.-W. Kim<sup>g</sup> G.-B. Kim<sup>q</sup> W.W. Kinnison<sup>1</sup> S. Klinksieck<sup>n</sup>  
L. Kluberg<sup>q</sup> H. Kobayashi<sup>u</sup> D. Koehler<sup>n</sup> L. Kotchenda<sup>s,w</sup>  
C.H. Kuberg<sup>a</sup> K. Kurita<sup>t</sup> M.J. Kweon<sup>j</sup> Y. Kwon<sup>z</sup> G.S. Kyle<sup>m</sup>  
J.J. LaBounty<sup>c</sup> J.G. Lajoie<sup>f</sup> D.M. Lee<sup>1</sup> S. Lee<sup>g</sup> M.J. Leitch<sup>1</sup>  
Z. Li<sup>t,d</sup> M.X. Liu<sup>1</sup> X. Liu<sup>c,d</sup> Y. Liu<sup>p</sup> E. Lockner<sup>n</sup> J.D. Lopez<sup>1</sup>  
Y. Mao<sup>t,d</sup> X.B. Martinez<sup>1</sup> M.C. McCain<sup>a</sup> P.L. McGaughey<sup>1</sup>  
S. Mioduszewski<sup>x</sup> R.E. Mischke<sup>1</sup> A.K. Mohanty<sup>b</sup>  
B.C. Montoya<sup>1</sup> J.M. Moss<sup>1</sup> J. Murata<sup>t</sup> M.M. Murray<sup>1</sup>  
J.L. Nagle<sup>e</sup> Y. Nakada<sup>k</sup> J. Newby<sup>x</sup> F. Obenshain<sup>o</sup>  
A.P.T. Palounek<sup>1</sup> V. Papavassiliou<sup>m</sup> S.F. Pate<sup>m</sup> F. Plasil<sup>o</sup>  
K. Pope<sup>x</sup> J.M. Qualls<sup>a</sup> G. Rao<sup>o</sup> K.F. Read<sup>o,x</sup> S.H. Robinson<sup>1</sup>  
G. Roche<sup>r</sup> A. Romana<sup>q</sup> P. Rosnet<sup>r</sup> R. Roth<sup>1</sup> N. Saito<sup>t,u</sup>  
T. Sakuma<sup>y</sup> W.F. Sandhoff, Jr.<sup>c</sup> L. Sanfratello<sup>n</sup> H.D. Sato<sup>k</sup>

R. Savino<sup>c</sup> M. Sekimoto<sup>h</sup> M.R. Shaw<sup>a</sup> T.A. Shibata<sup>y,t</sup>  
 K.S. Sim<sup>j</sup> H.D. Skank<sup>f</sup> D.C. Smith<sup>o</sup> G.D. Smith<sup>l</sup>  
 W.E. Sondheim<sup>l</sup> S. Sorensen<sup>x,o</sup> F. Staley<sup>v</sup> P.W. Stankus<sup>o</sup>  
 S. Steffens<sup>x</sup> E.M. Stein<sup>c</sup> M. Stepanov<sup>m</sup> W. Stokes<sup>c</sup>  
 M. Sugioka<sup>y,t</sup> Z. Sun<sup>d</sup> A. Taketani<sup>t</sup> E. Taniguchi<sup>y</sup> J.D. Tepe<sup>a</sup>  
 G.W. Thornton<sup>l</sup> W. Tian<sup>o,d</sup> J. Tojo<sup>k</sup> H. Torii<sup>k</sup> R.S. Towell<sup>a,l</sup>  
 J. Tradeski<sup>c</sup> M. Vassent<sup>r</sup> C. Velissaris<sup>m</sup> L. Villatte<sup>x</sup> Y. Wan<sup>d</sup>  
 Y. Watanabe<sup>t,u</sup> L.C. Watkins<sup>o</sup> B.R. Whitus<sup>o</sup> C. Williams<sup>o</sup>  
 P.S. Willis<sup>a</sup> B.G. Wong-Swanson<sup>l</sup> Y. Yang<sup>c,d</sup> S. Yoneyama<sup>y</sup>  
 G.R. Young<sup>o</sup> S. Zhou<sup>d</sup>

(The PHENIX Collaboration)

<sup>a</sup>*Abilene Christian University, Abilene, TX 79699, USA*

<sup>b</sup>*Bhabha Atomic Research Center, Bombay 400 085, India*

<sup>c</sup>*Brookhaven National Laboratory, Upton, NY 11973, USA*

<sup>d</sup>*China Institute of Atomic Energy (CIAE), Beijing, People's Republic of China*

<sup>e</sup>*Columbia University, New York, NY 10027 and Nevis Laboratories, Irvington,  
 New York 10533, USA*

<sup>f</sup>*Iowa State University, Ames, IA 50011, USA*

<sup>g</sup>*Kangnung National University, Kangnung, 210-702, Korea*

<sup>h</sup>*KEK, High Energy Research Accelerator Organization, Tsukuba-shi, Ibaraki-ken  
 305-0801, Japan*

<sup>i</sup>*C.A.L., Korea Cancer Hospital, Seoul, 139-706, Korea*

<sup>j</sup>*Korea University, Seoul, 136-701, Korea*

<sup>k</sup>*Kyoto University, Kyoto 606, Japan*

<sup>l</sup>*Los Alamos National Laboratory, Los Alamos, NM 87545, USA*

<sup>m</sup>*New Mexico State University, Las Cruces, NM 88003, USA*

<sup>n</sup>*University of New Mexico, Albuquerque, NM 87131, USA*

<sup>o</sup>*Oak Ridge National Laboratory, Oak Ridge, TN 37831, USA*

<sup>p</sup>*I.P.N., BP 1, 91406 Orsay, France*

<sup>q</sup>*L.L.R., Ecole Polytechnique, 91128 Palaiseau, France*

<sup>r</sup>*L.P.C., Universite Blaise Pascal, 63177 Aubiere Cedex, France*

<sup>s</sup>*Petersburg Nuclear Physics Institute, Gatchina, 188350, Russia*

<sup>t</sup>*RIKEN (The Institute of Physical and Chemical Research), Waco, Saitama  
 351-0198, Japan*

<sup>u</sup>*RIKEN BNL Research Center, Brookhaven National Laboratory, Upton, NY*

11973, USA

<sup>v</sup>DSM/Daphnia/SPhN, CEA/Saclay, 91191 Gif-sur-Yvette Cedex, France

<sup>w</sup>State Interphysica, Protvino, Russia

<sup>x</sup>University of Tennessee, Knoxville, TN 37996, USA

<sup>y</sup>Department of Physics, Tokyo Institute of Technology, Tokyo 152-8551, Japan

<sup>z</sup>Yonsei University, IPAP, Seoul 120-749, Korea

The PHENIX Muon Arms detect muons at rapidities of  $|y|=(1.2-2.4)$  with full azimuthal acceptance. Each muon arm must track and identify muons and provide good rejection of pions and kaons ( $\sim 10^{-3}$ ). In order to accomplish this we employ a radial field magnetic spectrometer with precision tracking (Muon Tracker) followed by a stack of absorber/low resolution tracking layers (Muon Identifier). The design, construction, testing and expected run parameters of both the muon tracker and the muon identifier are described.

## 1 Introduction

The Relativistic Heavy Ion Collider (RHIC) accelerates beams from protons to gold reaching energies of 100 GeV/nucleon for the heaviest beams. The PHENIX experiment [1] probes several fundamental features of the strong interaction. A prime goal for experiments with heavy ion beams is to produce a deconfined state of nuclear matter called the Quark Gluon Plasma (QGP) and study its properties. Study of muons that have minimum interaction with the hot hadronic matter produced in central collisions probes the QGP phase directly. RHIC also provides an opportunity to study collisions of polarized protons at beam energies up to 250 GeV. The aim is to measure the spin structure of the nucleon.

In order to carry out this broad physics agenda the PHENIX detector utilizes a variety of detector technologies including global detectors, a pair of central spectrometers at mid rapidity to measure electrons, hadrons and photons, and a pair of forward spectrometers to measure muons. Each muon spectrometer has a large geometric acceptance of about one steradian and excellent momentum resolution and muon identification. The PHENIX Muon Arms provide a means of studying vector meson production, the Drell-Yan process (via the detection of muon pairs) and heavy quark production. Z and W production will be studied at forward rapidities (via the detection of single high- $P_T$  muons). Detection of Z and W particles produced by collisions of polarized protons will be important in determining the contribution of gluons to the proton spin.

Each muon arm consists of a muon tracker followed by a muon identifier. A discussion of the muon tracker followed by a discussion of the muon identifier is given below.

## 2 The Muon Tracker

The Muon Arm Tracker design specifications were driven by the requirements that it be able to 1) allow a clean separation of  $J/\psi$  from  $\psi'$ ,  $\Upsilon(1S)$  from  $\Upsilon(2S,3S)$  and  $\rho/\omega$  from  $\phi$ , 2) provide a large enough signal-to-background and acceptance for vector mesons to be able to do statistically significant physics measurements in less than 1 year of RHIC running, 3) have low enough occupancy to be able to reconstruct tracks efficiently in central Au-Au events and 4) still perform well in the lower occupancy but higher event rate p-p and p-A physics programs.

The relative mass resolution is approximately given by  $\sigma(M)/M = 6\%/\sqrt{M}$ , where  $M$  is in GeV. This mass resolution enables a clear separation of the  $\rho/\omega$  peak from the  $\phi$ ,  $J/\psi$  and  $\psi'$ , with an acceptable separation of  $\Upsilon$  and  $\Upsilon'$ . This is consistent with a spacial resolution of 100 microns.

The above design requirements led to a Muon Tracker design which is comprised of three stations of cathode-strip readout tracking chambers mounted inside conical-shaped muon magnets (see Fig. 1), with multiple cathode strip orientations and readout planes in each station. The muon magnet is described in great detail in the paper on PHENIX magnets[2] elsewhere in this volume. The electronics design specifications were driven by the requirement that the non-stereo cathode planes provide 100  $\mu\text{m}$  resolution measurements of the particle trajectories and that the readout of the system be able to meet the global PHENIX readout requirements. Test-bench measurements from production chambers and electronics combined with simulations of the full muon tracker design show that the tracker should meet the design requirements outlined above.

### 2.1 Mechanical Design

Each of the three stations of cathode strip chambers (CSC) presented unique design requirements. All are in the shape of octants built with a 3.175 mm half gap, 5 mm cathode strips and with alternate strips readout. For the mechanical construction, honeycomb technology was used for stations 1 and 3 and thin foil technology for station 2. Each station used a specific technology to produce a cathode pattern to an accuracy of better than 25 microns; station

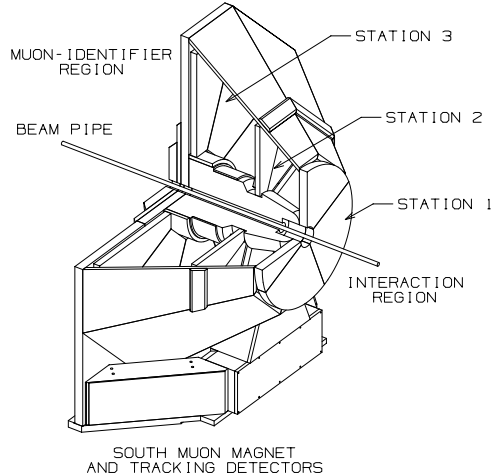


Fig. 1. The South Muon ARM tracking spectrometer. Muons from the intersection region, to the right, intercept the station 1, 2 and 3 detectors and proceed to the muon identifier detectors to the left (not shown).

Station 1 used photolithography, station 2 used electro-mechanical etching at a facility designed specifically for this purpose and station 3 used mechanical routing. A unique wire laying apparatus was designed and implemented for each station. The anode planes are alternating structures of  $20\ \mu\text{m}$  gold-plated W sense wires and  $75\ \mu\text{m}$  gold-plated Cu-Be field wires with a sense wire spacing of 10 mm. Half of the cathode planes have strips perpendicular to the anode wires and the other half have strips at stereo angles between  $0$  and  $\pm 11.25$  deg with respect to the perpendicular strips. The chamber gas mixture is  $50\% \text{ Ar} + 30\% \text{ CO}_2 + 20\% \text{ CF}_4$  with a gas recirculation system included in normal operation. The typical operating conditions for this gas are that the HV is 1850 V with a gain of approximately  $2 \times 10^4$ . The charge deposited by a minimum ionizing particle in the CSC is assumed to be 100 electrons. This results in a total cathode charge of 80 fC. This is an average and the charge is Landau distributed.

The station 1 tracking chambers are located closest to the interaction region and therefore are the smallest (approximately 1.25 m from inside radius to outside radius), have the highest occupancy per strip, and the most stringent requirements on dead regions within the acceptance ( $\geq 95\%$  active area). The chambers are constructed in quadrants using honeycomb panels laminated with photo-etched copper clad FR-4 to produce the cathode strips (see Fig. 2). The quadrant consists of three chamber gaps, each containing a pair of cathode strip planes on either side of an anode wire plane.

Because of the need to maintain good momentum resolution down to 1.5 GeV, the thickness at the station 2 detector was required to be  $\leq 0.1\%$  of a radiation length. To meet this requirement, the station 2 octant cathodes were made of etched 25 micron copper coated mylar foils. The thickness of the copper coat is 600 Angstroms. The 6 cathode foils as well as the 3 anode wire planes are

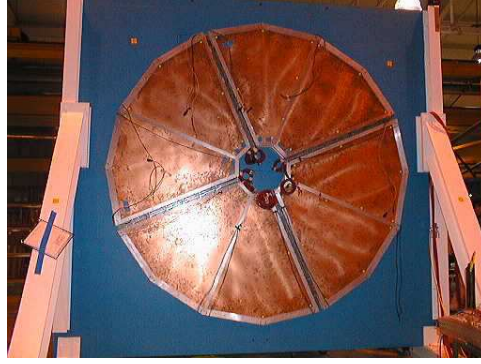


Fig. 2. Station 1 is built in four quadrants but is electrically divided into octants to match the octants of station 2 and station 3.



Fig. 3. This octant from station 2 has six cathode foils and three anode wire planes. The total thickness is  $8.5 \times 10^{-4}$  radiation lengths.

made of thin 3.175 mm laminated frames. The station 2 design is a laminated structure of these thin anode and cathode frames held under tension by two thick aluminum support frames. Aluminized mylar windows contain the gas mixture and the three separate CSC detectors are isolated by ground foils. The station 2 octant is shown in Fig. 3. The frame is approximately  $1.9 \times 1.7 \text{ m}^2$  and the active area is the same to this degree of accuracy. The total thickness is  $8.5 \times 10^{-4}$  radiation lengths.

Station 3 chambers are the largest of the tracking chambers with each of the octant chambers about 2.4 m long and 2.4 m wide (Fig. 4). Like station 1, these chambers are constructed using honeycomb panels that are laminated with copper clad FR-4 sheets. The cathode strips are formed by mechanically routing shallow lines in the copper skin. These chambers consist of two gaps, each containing a pair of cathode readout planes on either side of an anode wire plane.



Fig. 4. This octant from station 3 is 2.4 m long and 2.4 m wide and consists of four planes of cathode strips on honeycomb panels and two anode wire planes.

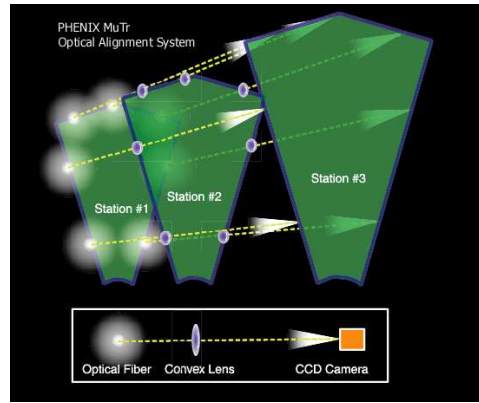


Fig. 5. Optical Alignment System in which light from an optical fiber is projected from station 1 through station 2 to a CCD mounted on station 3. The relative chamber positions are monitored to  $\pm 25 \mu\text{m}$

To maintain the momentum resolution, an optical alignment system is installed to calibrate initial placement of the chambers, and to monitor displacements of the chambers to  $\pm 25 \mu\text{m}$  (Fig. 5). There are seven optical beams surrounding each octant chamber, consisting of an optical fiber light source at station 1, a convex lens at station 2 and a CCD camera at station 3.

## 2.2 Electronics Design

The Muon Tracking Front End Electronics (FEE) is the interface between the muon chambers and the PHENIX online Data Acquisition (DAQ) system [3]. The electronics continuously amplifies and stores analog hit information from the chamber cathodes. Upon receipt of a level 1 trigger from the PHENIX granule timing module (GTM), stored samples from all channels are digitized and the results are sent to the PHENIX data collection module (DCM).

To meet the design requirement of  $100 \mu\text{m}$  resolution, the rms noise at the

input to the preamps was required to be 0.5 fC ( $3125 e^-$ ) for a typical pulse of 80 fC. This is for a preamp with 3.5 mV/fC and a dynamic range of 11 bits.

Space constraints precluded placing the electronics directly on the chambers so 60 cm (45 cm for station 1) cables connect the FEE's to the chambers. The electronics is modular. Two types of 6U size boards are contained in custom chassis. The chassis includes water cooled side plates and a backplane for communication between boards. The Cathode Readout Card (CROC) includes 64 channels of preamplifiers (8 Cathode Preamp (CPA) chips with 8 channels each) and two Analog Memory Unit/Analog to Digital Converters (AMUADC's). These two ASIC's were designed at Oak Ridge National Laboratory (ORNL) [4]. The performance of the CROC board is detailed in [5]. The ADC clock is 200 MHz so for 11 bit accuracy, 4 samples can be converted within the time constraint of 40  $\mu$ sec per event. Up to five events can be converted and stored locally to be transferred to the PHENIX DAQ. The Control board includes the ARCNet interface (a network connection which permits downloading of FEE settings), the Field Programmable Gate Array (FPGA) to control the AMUADC's, and transmitters and receivers for the GTM and DCM information.

A platform mounted on top of the magnet supports three electronics racks. These contain the high voltage power supplies for the chambers, the low voltage power for all the electronics, interfaces for fiber optics from the PHENIX counting house, calibration electronics, and auxiliary controls and monitoring. A common set of FEE's for the PHENIX detector is described elsewhere in this volume[3].

Fast timing signals carried on optical fibers (GLink) are translated to copper wires (CLink) just outside the magnet and transported to the chassis via 7 m cables. Similarly, outgoing data packets travel on cables to the CLink/Glink interface and then to the data collection modules in the counting house on optical fibers. A separate system, called ARCNet is used for slow controls information to the chassis and the GLink/CLink crates. Important functions of this system include downloading serial string information to the CPA, AMUADC, and FPGA chips to set operating parameters, the interface to temperature, voltage, and current monitors, and the ability to remotely download the FPGA code.

A calibration system has been implemented to inject pulses into all of the chambers. Four wires in each chamber gap, which span the entire width of the cathode planes, are sent a square pulse from a digital to analog converter (DAC) thus inducing a charge on all cathode strips in a given gap simultaneously. Several different pulse amplitudes are sent to the chambers and many events are collected at each amplitude so that the relative gains of the cathode strips can be determined over the entire range of the electronics. The pedestals

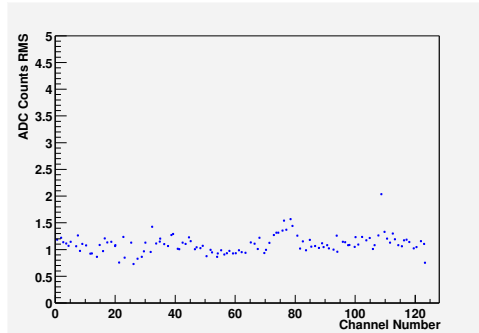


Fig. 6. RMS noise measurement for 128 typical channels in units of ADC counts (1 ADC count  $\sim$  2 mV) obtained in cosmic-ray tests of the station 2 octant.

are monitored by collecting calibration data with the DAC amplitude set to zero.

### 2.3 Integrated Performance

Integrated performance of the production chambers and electronics has been studied in a cosmic-ray test with one station 2 chamber and its full complement of electronics, and in readout of the entire South Muon Tracker system prior to the year 2001 RHIC run. The cosmic-ray test data showed that the system was capable of meeting the noise specifications and that 100  $\mu$ m resolution could be achieved with the station 2 chamber. The noise specifications have now been met on the full south muon tracker system and the system has been shown to be robust over several months of data taking. The current readout system is very close to design specifications, capable of doing 4-sample ADC conversions within 50  $\mu$ sec and holding up to 4 events worth of data in FEE buffers. The goal of the next version of the FPGA program is to meet the PHENIX readout design specifications, i.e., perform ADC conversions within 40  $\mu$ sec time budget and store up to 5 events in the buffer. The FPGA code can be updated remotely at any time through an ARCnet serial download.

The cosmic-ray test was performed with one station 2 chamber, 960 channels of production FEE's, the same high-voltage and low-voltage distribution system that is used in the final system, and with a copy of the PHENIX DAQ system. The noise specifications of 0.5 fC were met, as can be seen in Fig. 6, where the RMS values of the pedestals on all readout channels are shown.

Two scintillators, one on either side of the station 2 chamber, were used to provide a trigger for cosmic rays going through the chamber. The data collected from this trigger were searched for clusters in each cathode readout plane, the clusters were fit to extract the centroid strip positions, and 5 out of 6 of the readout planes were fit to a straight line and projected to the

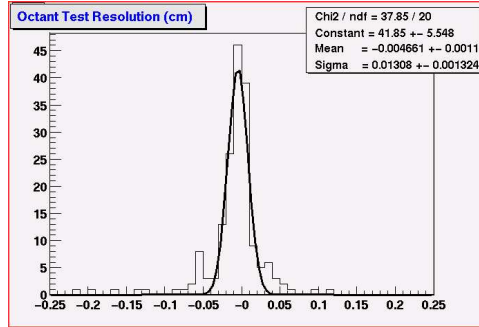


Fig. 7. Measurement of position resolution obtained in cosmic-ray tests of a station 2 octant. The composite chamber plus projection error was about  $131 \mu\text{m}$ , consistent with the  $100 \mu\text{m}$  specification for the chambers and readout alone.

sixth, central non-stereo readout plane. A cut was placed on the straight line fit to only select tracks which were approximately perpendicular to the face of the chamber and the difference between the projected straight-line fit and the measured position on the sixth plane was plotted. The result is shown in Fig. 7, where a resolution of approximately  $100 \mu\text{m}$  was achieved when the projection error is removed from the residual.

The entire South Muon Tracker system was installed in the Muon magnet in the PHENIX Assembly Hall late in the year 2000. The complete installation and shakedown of the FEE system was completed in late January 2001. The entire readout chain from cathodes strips through the DAQ system was also studied with the calibration system. Each individual channels' gain, pedestal and variation (or noise) in the pedestal was measured. The dynamic range in the charge measurement of the system was verified and long runs demonstrated the stability of the FEM's optical links. Fig. 8 shows the residuals from a gain measurement during the commissioning period. The residuals are shown to be consistent with a linear gain to a few ADC counts over the operable ADC range.

Monitoring of the electronics temperature is an important issue since the muon FEE's will operate inside the closed magnet for an extended period of time and some of the electronics components are sensitive to temperature. The slow control system based on the ARCNet protocol has proven to be able to monitor all the crate temperatures. Also the water-cooling system, which can carry away enough heat to keep the electronics in normal operational mode, has been exercised extensively in the assembly hall.

The full array of muon cathode-strip chambers has been tested up to the nominal high voltage (1700 VDC) in place in the magnet. The optical alignment system is fully installed and images are seen on all the cameras. The South magnet has had all lampshade panels installed, and the magnet has been moved into place near the intersection region. The detection of the first  $J/\psi$ 's at RHIC is expected soon after the beam turns on for the year 2001

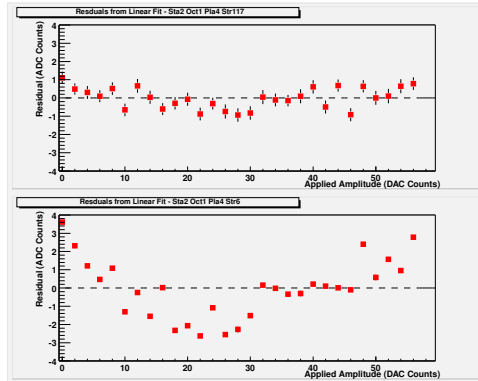


Fig. 8. Plotted are the residuals (in ADC counts) from a straight-line fit to the charge measured on a given strip of the ADC vs the DAC pulse amplitude applied to the calibration wires. Two different strips from a given cathode plane are shown. Approximately one half of the ADC range (of 2047 channels) is shown and is linear to a few ADC counts and constant over time.

PHENIX run.

### 3 The Muon Identifier

The irreducible  $\mu/\pi$  ratio due to weak decay before the nosecones inside PHENIX is approximately  $1 \times 10^{-3}$  (primarily determined by the proximity of the nosecone to the vertex). We set a detector design criteria to  $1/4$  of this, namely  $2.5 \times 10^{-4}$ , for a pion from the vertex (or a hadronic descendant) to be misidentified as a muon (forming part of a dimuon). The factor of  $1/4$  provides over an order of magnitude suppression for the *pair* background. Thus, the irreducible background of muons reaching the muon identifier (MuID), as opposed to the MuID design and the algorithms used to reject the larger hadron background, will set the ultimate physics background level. Of this required net  $\mu/\pi$  separation, approximately  $10^{-2}$  is provided by the presence of steel preceding the MuID which filters out pions. This leaves 3% as the maximum tolerable fraction of the charged pions which may subsequently be misidentified as muons.

In order to set the punch-through probability for pions of up to 4 GeV/c to be 3% or less, a total steel depth of 90 cm (5.4 hadronic interaction lengths) is required beyond the nosecone and central magnet. Subtracting the thickness of the muon magnet backplate, a total depth of 60 cm of steel is required in the MuID itself. A muon at the vertex must have a mean energy of at least 1.9 GeV to reach the MuID system. The mean minimum original energy for a muon to penetrate completely through the MuID is 2.7 GeV.

### 3.1 Detector Design

Segmentation of the absorber into multiple layers improves the measurement of the trajectory in the MuID. It is desirable to have the early absorber layers be divided more finely to increase the acceptance for  $\phi$  meson detection. The segmentation chosen is a total of four steel absorbers after the 30 cm thick muon magnet backplate of the north arm of thicknesses 10, 10, 20, 20 cm. The 5 gaps created by the absorbers are instrumented with the MuID panels. The MuID for the south arm is identical to that for the north arm (although the muon magnet backplate is only 20 cm thick) and at the same distance from the interaction vertex.

Iarocci tubes[6] were chosen as the detector technology. We use the term Iarocci tubes to refer to planar drift tubes consisting of 100- $\mu$ m gold-coated CuBe anode wires at the center of long channels of a graphite-coated plastic cathode. This same physical detector when operated at higher voltage is a conventional limited streamer tube. We operate them in the proportional mode to increase longevity. They have proven reliability and longevity, compactness, low cost, and are readily available from commercial vendors. Such tubes can be used economically to tile large areas. They have robust wires and seals and they avoid the problems of metal-plastic transitions present at the endcaps for aluminum proportional tubes.

Standard commercially-available Iarocci tubes have a width of 8.4 cm. Beam gas studies show that for low polar angles ( $20^\circ$  or less), an effective segmentation into logical pads of approximately 13 by 13 cm is required to suppress false roads for tracks in the muon identifier. Rather than develop Iarocci tubes of greater width or use 13 cm wide external strips, the most cost effective solution is simply to use standard-width 8.4 cm tubes with all eight internal wires ganged together. This provides a readout pitch of 8.4 cm along both the  $x$  and  $y$  directions, thus providing effective 8.4 cm square hodoscopic cells (upon forming the appropriate ANDs). This most cost effective solution exceeds our requirements. This segmentation is fine enough to provide sufficient granularity for matching roads in the identifier to tracks in the muon tracker unambiguously with anticipated occupancies.

Tubes with 9 mm by 9 mm channels satisfy the count-rate and position localization requirements, but must be staggered by half a cell and OR'd in pairs (discussed below) to meet the timing requirements of the Local Level 1 (LVL-1) trigger system.

An individual anode wire and the immediately surrounding gas volume and graphite-coated walls are referred to as one channel of an Iarocci tube. There are 8 such wires in a tube. Each wire is held at the center of its channel by



Fig. 9. Muon identifier panel being flipped over during construction.

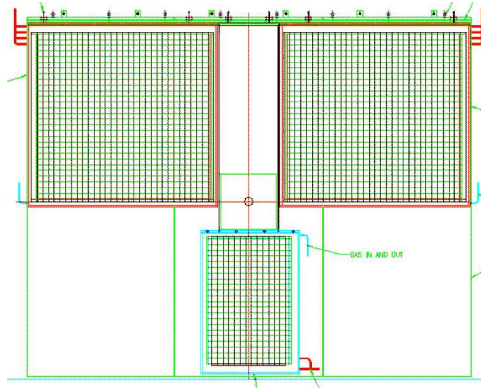


Fig. 10. Design drawing showing panels A, C, and E in a typical gap.

means of plastic wire spacers positioned every 50 cm along the tube. A two-pack is a pair of tubes connected together and staggered by half a channel. Their signals are OR'd together. Groups of two-packs oriented both horizontally and vertically are held inside an aluminum box. (See Fig. 9.) Approximately half are oriented horizontally and half are oriented vertically so that both projections are measured. This total detector element is called a muon identifier panel. There are six such panels per gap labelled A through F (counterclockwise from the upper left) arranged around the square hole left for the beam pipe to pass through. The large panels A, C, D, F are located at the 4 corners of the gap. Each contains 118 horizontal tubes of length 5200 mm and 128 vertical tubes of length 5010 m. The small panels B and E are situated above and below the square hole, respectively. Each contains 90 horizontal tubes of length 2504 mm and 52 vertical tubes of length 3821 mm. In this way, 1268 tubes per gap (6340 tubes per arm) are distributed to tile an area of 13.1 m wide by 10.7 m high in each gap. Adjacent panels overlap along their edges to eliminate deadspace.

Panels A, C, and E (Fig. 10) lie in one plane which is 10 cm closer to the vertex than the plane of the other panels (B, D, and F). The acceptance reaches down to  $10^\circ$  in the first plane (and even farther in subsequent planes) except immediately at the four corners of the square beam hole. Fig. 11 shows



Fig. 11. The south PHENIX Muon Identifier before installation of the shield wall.

the panels as installed in the south arm of PHENIX.

The MuID planes need not be surveyed with respect to the vertex to better than approximately  $\pm 4$  mm in the  $x$  and  $y$  directions in order to have alignment errors be negligible compared to multiple scattering errors. It is only required that the  $z$  positions be measured after they are installed, and this measurement only has to be known to within a few centimeters relative to the vertex.

The MuID has two separate gas volumes. The primary one is the tube gas volume. The secondary volume is the aluminum enclosure of each panel surrounding the primary volume. A mixture of  $CO_2$  and up to 25%  $i-C_4H_{10}$  is fed into the primary volume for chamber operation.  $N_2$  is fed into the secondary volume in order to keep the chamber electronics dry and clean, and to dilute the flammable gas component in the case of a primary volume leak. There are a total of 600 gas circuits for the primary volume. The total sizes of the primary and secondary volumes are  $50\text{ m}^3$  and  $40\text{ m}^3$ , respectively. The gas flow rate of the primary volume is one volume exchange per day. The gas supply system can recirculate up to 50% of the flow of the primary volume.

### 3.2 Readout

We have chosen to operate the Iarocci tubes in proportional mode to ensure maximum longevity at 4500 V. To ensure adequate signal-to-noise performance in the unknown noise environment at RHIC we settled on a readout scheme that employs in-panel amplification (x150) driving differential signals on 30 m twisted-pair cables to a crate-based processing system. Here the signals must be digitized and synchronized such that all signals from a beam crossing arrive simultaneously (a significant challenge given the inherent differences in drift-time, transmission time down the 5m tubes and large slew for near-threshold hits). Data from every crossing is sent as the muon arm input to the LVL1 trigger. Trigger latency (for all beam crossings) and read-

back latency (for LVL1-accepted crossings), required to satisfy the PHENIX pipelined/deadtime-less specification, is provided locally.

The anodes from two half-cell staggered Iarocci tubes are capacitively coupled into the amplifier circuit, thus comprising a readout channel. In addition to signal amplification, the in-panel portion of the electronics must distribute high voltage to the tubes. Six readout channels are mounted on a  $8.2 \times 50.4 \text{ cm}^2$  printed circuit board. Different channels share power, HV buses and a pulser circuit. The amplification circuit and HV distribution circuit are mounted on opposite sides of the board so that the HV can be isolated from human contact. The boards are mounted inside the panels at the tube endcaps. The primary requirement for the in-panel portion of the electronics was longevity.

The amplification circuit was based on an L3 design with several features incorporated to improve longevity: 1) Resettable polyfuses on the power inputs of each channel, 2) A double-diode protection circuit that allows an amplifier channel to survive even after one of its input tubes has broken a wire, and 3) Diode clamps to prevent reverse-bias damage. Furthermore, the HV input for each tube has a  $400 \text{ M}\Omega$  current-limiting resistor so that the HV for the circuit will continue to operate with multiple tube failures and all HV components are encapsulated in a silicone conformal coating to enhance longevity and safety.

In addition to these steps, we have maintained a design in which different tube planes are on independent separate gas and HV circuits and each plane is further segregated into roughly 24-channel HV, gas and power segments.

The out-panel (post-amplifier) electronics are housed in a set of four 9U crates, each of which has two types of cards (ROC's and FEM's), described below, as well as transition cards to bring in signals and a custom backplane for communication between ROC's and FEM's.

The FEM cards are analagous to a conventional crate controller, providing the interfaces between the MuID and the PHENIX online systems (with the exception of LVL1). The timing and control interface receives mode bit information and uses a state machine to parse the instructions, validate them and route them to the appropriate places. Upon receipt of a LVL1-accept signal the DCM interface assembles and ships out the data from all ROC's in the crate.

The ROC cards consist of analog processing and synchronization, buffering, supplemental diagnostics and serial control. The first stage of the analog processing chain is a differential receiver for the input signals which converts the signals to single-ended and amplifies them by a factor of 3. The signals then go through a novel delay-less constant-fraction discriminator to eliminate small-signal slew Synchronization is obtained in stages through a series of programmable delays and multiplexers that allow the operator to select the

Table 1  
 Simulated performance of the MuID.

p (GeV/c)	$\mu$ Effic. (%)	$\pi$ Rejection Rate
2.0	$65.3 \pm 1.1$	$(2.0 \pm 1.4) \times 10^{-4}$
3.0	$93.7 \pm 1.4$	$(2.3 \pm 0.5) \times 10^{-3}$
4.0	$96.9 \pm 1.4$	$(2.5 \pm 0.5) \times 10^{-3}$
5.0	$98.1 \pm 1.4$	$(3.7 \pm 0.6) \times 10^{-3}$
10.0	$99.6 \pm 1.4$	$(3.9 \pm 0.7) \times 10^{-3}$

optimal clock phase for each channel (by delaying the clock and not the channel we can exchange delay lines for multiplexers, greatly reducing the cost of the system). With this scheme we can synchronize all channels if the following two restrictions are met: 1) all signals coming into a ROC must arrive within one RHIC cycle (106 ns), and 2) the earliest signals into all ROC's must arrive within one RHIC cycle.

### 3.3 Level-1 Trigger

Each MuID ROC sends 96 bits of data to the LVL1 trigger system (discussed elsewhere in this volume) [3] where an algorithm is implemented to determine if there are candidate muon tracks in the event. The algorithm finds roads pointing towards the vertex. It allows missed gaps along the road and phrases its requirements in terms of the number of deep or shallow roads in each orientation. The algorithm is “steerable” from gap to gap, meaning that the roads can vector based on the hit pattern in the two preceding gaps. The LVL-1 trigger efficiency is flat as a function of rapidity over almost the entire acceptance.

### 3.4 Detector Performance

Single-muon events were simulated and reconstructed to check the reconstruction efficiency of the MuID. Single-pion events were simulated to estimate the hadron rejection capability as well. The performance of the MuID in high multiplicity was also investigated by mixing  $J/\Psi$  signal events with central Au-Au background events.

The results shown in Table 1 indicate an overall muon efficiency of about 65% to 99% from 2.0 to 10.0 GeV/c, and a pion rejection rate of about  $2.0 \times 10^{-4}$

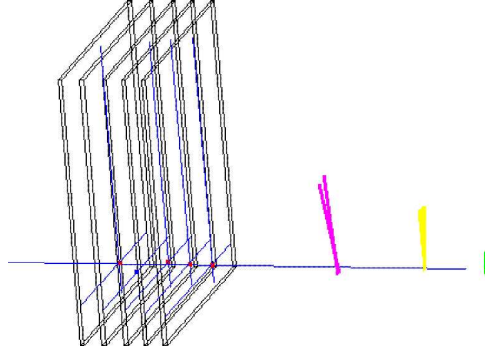


Fig. 12. Cosmic ray track in the south muon arm.

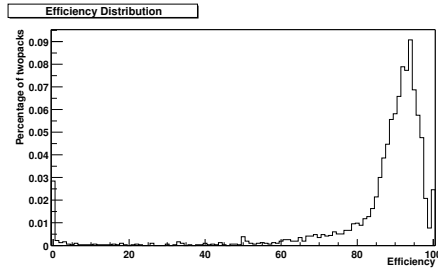


Fig. 13. Efficiencies for two-packs in the south MuID.

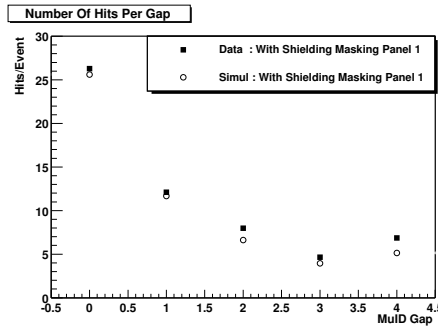


Fig. 14. Total occupancy per gap in the MuID for data versus simulation.

to  $3.9 \times 10^{-3}$  in the same momentum region. The lower efficiency at 2.0 GeV/c is due to the energy loss caused by the central magnet and MuID absorber. The pion rejection rate indicated in this table is the fraction of simulated pions which satisfy the criteria for being considered a muon candidate. This rate includes the irreducible contribution from decay muons which come from pions. The portion of this rate not due to decay muons is consistent with the design goal of  $2.5 \times 10^{-4}$ . The numbers in Table 1 are consistent with the result from our test experiment in KEK with 1.5-4.0 GeV/c pion/muon beam.

After an initial engineering run during summer 2000, we commissioned the entire south MuID in the summer of 2001. Initially, we collected cosmic ray data. Fig. 12 shows a cosmic ray track detected in the south muon arm. Using cosmic ray data we were able to make an initial measurement of the tube efficiencies (Fig. 13).

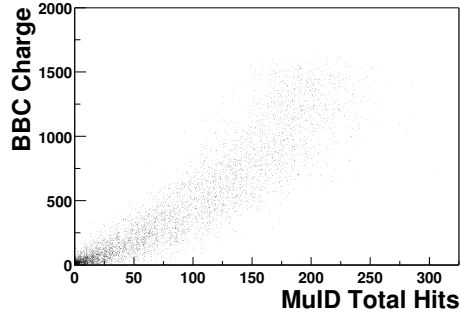


Fig. 15. Beam-beam counter charge sum versus number of hits in the muon identifier.

During initial data collection with Au-Au collisions, beam-related backgrounds were observed in the MuID requiring shielding inside the square hole. Fig. 14 shows the occupancy measured in each gap of the MuID after installation of the shielding (and masking off the panels above the beam pipe which could not be shielded immediately). The measured occupancy agrees closely with simulation gap-by-gap.

Fig. 15 shows the total charge measured in the PHENIX beam-beam counter versus the total occupancy in the MuID. The strong correlation shows that the MuID hits are due to beam collisions.

## 4 Summary

The design goals and key aspects of construction of the PHENIX muon arms have been described. The south muon arm was constructed and commissioned in time for operation during the 2001-2 RHIC run. The north muon arm construction and commissioning will be complete in time for the run beginning in late 2002. Tests and initial results indicate that the demonstrated performance is consistent with expectations from simulations.

## 5 Acknowledgements

We gratefully acknowledge the efforts of the RHIC staff. This work was supported by grants from the U.S. Department of Energy's Nuclear Physics Division, the Japanese Ministry of Education Culture, Sports, Science and Technology (Monbukagakusho) and the French IN2P3/Centre National de la Recherche Scientifique and DAPNIA/Commissariat a l'Energie Atomique.

## References

- [1] Article entitled “PHENIX Detector Overview” this volume.
- [2] Article entitled “PHENIX Magnet System” this volume.
- [3] Article entitled “PHENIX On-Line Systems” this volume
- [4] M.S. Emery et al., “Muon Tracker Preamp User’s Data Sheet,” Oak Ridge National Laboratory, December 1988; M.S. Emery et al., *IEEE Trans. Nucl. Sci.* **44**, (1997) 374.
- [5] M.M. Cafferty et al., Nuclear Science Symposium, IEEE, 1999, 2, (1999) 765.
- [6] E. Iarocci, *Nucl. Instr. and Meth.* 217 (1983) 30.